

LEVEL II

12

AD A092919

**Precipitation of Inner-Zone Electrons
by Whistler-Mode Waves from the VLF Transmitters
UMS and NWC**

H. C. KOONS, B. C. EDGAR and A. L. VAMPOLA
Space Sciences Laboratory
Laboratory Operations
The Aerospace Corporation
El Segundo, Calif. 90245

1 December 1980

SD DTIC ELECTE D
DEC 15 1980
E

Interim Report

APPROVED FOR PUBLIC RELEASE;
DISTRIBUTION UNLIMITED

DDC FILE COPY

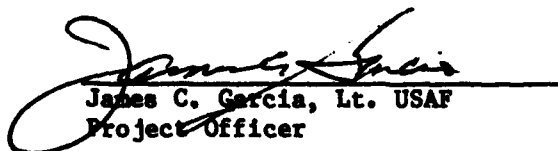
Prepared for
SPACE DIVISION
AIR FORCE SYSTEMS COMMAND
Los Angeles Air Force Station
P.O. Box 92960, Worldway Postal Center
Los Angeles, Calif. 90009

80 12 15 037

This interim report was submitted by the Aerospace Corporation, El Segundo, CA 90245, under Contract No. F04701-80-C-0081 with the Space Division, Deputy for Technology, P.O. Box 92960, Worldway Postal Center, Los Angeles, CA 90009. It was reviewed and approved for The Aerospace Corporation by G. A. Paulikas, Director, Space Sciences Laboratory. Lieutenant James C. Garcia, SD/YLXT, was the project officer for Technology.

This report has been reviewed by the Public Affairs Office (PAS) and is releasable to the National Technical Information Service (NTIS). At NTIS, it will be available to the general public, including foreign nations.

This technical report has been reviewed and is approved for publication. Publication of this report does not constitute Air Force approval of the report's findings or conclusions. It is published only for the exchange and stimulation of ideas.


James C. Garcia, Lt. USAF
Project Officer


Joseph J. Cox, Jr., Lt Col, USAF
Chief, Advanced Technology Division

FOR THE COMMANDER


Burton H. Holaday, Col, USAF
Director of Space Systems Planning
Deputy for Technology

UNCLASSIFIED

SECURITY CLASSIFICATION OF THIS PAGE (When Data Entered)

19) REPORT DOCUMENTATION PAGE		READ INSTRUCTIONS BEFORE COMPLETING FORM	
1. REPORT NUMBER SD-TR-80-76	2. GOVT ACCESSION NO. AD-A092 929	3. RECIPIENT'S CATALOG NUMBER	
4. TITLE (and Subtitle) PRECIPITATION OF INNER-ZONE ELECTRONS BY WHISTLER-MODE WAVES FROM THE VLF TRANSMITTERS UMS AND NWC.		5. TYPE OF REPORT & PERIOD COVERED Interim Rpt. /	
7. AUTHOR(s) H. C. / Koons, B. C. / Edgar and A. L. / Nampola		6. PERFORMING ORG. REPORT NUMBER TR-0081(6960-05)-6	
9. PERFORMING ORGANIZATION NAME AND ADDRESS The Aerospace Corporation El Segundo, Calif. 90245		8. CONTRACT OR GRANT NUMBER(s) F04701-80-C-0081 NSF-ATM 77-28207	
11. CONTROLLING OFFICE NAME AND ADDRESS Space Division Air Force Systems Command Los Angeles, Calif. 90009		10. PROGRAM ELEMENT, PROJECT, TASK AREA & WORK UNIT NUMBERS 12) 47	
14. MONITORING AGENCY NAME & ADDRESS (if different from Controlling Office)		12. REPORT DATE 1 Dec 80 /	
		13. NUMBER OF PAGES 47	
		15. SECURITY CLASS. (of this report) Unclassified	
		15a. DECLASSIFICATION/DOWNGRADING SCHEDULE	
16. DISTRIBUTION STATEMENT (of this Report) Approval for public release; distribution unlimited			
17. DISTRIBUTION STATEMENT (of the abstract entered in Block 20, if different from Report)			
18. SUPPLEMENTARY NOTES			
19. KEY WORDS (Continue on reverse side if necessary and identify by block number) Whistler-mode VLF Wave-particle interactions Radiation belt Electron precipitation			
20. ABSTRACT (Continue on reverse side if necessary and identify by block number) The precipitation of energetic electrons which are commonly observed in the drift loss cone east of 60° longitude between L ~ 1.6 and L ~ 1.8 can be accounted for by a doppler-shifted cyclotron resonance between the electrons and nonducted whistler-mode waves from high-power, ground-based VLF transmitters. A ray-tracing analysis using a diffusive-equilibrium model shows that 17.1 kHz waves starting with vertical wave normals between 23 and 31° magnetic latitude cross the magnetic equator between L ~ 1.6 and L ~ 1.8 with wave			

DD FORM 1473
(FACSIMILE)

UNCLASSIFIED

SECURITY CLASSIFICATION OF THIS PAGE (When Data Entered)

UNCLASSIFIED

SECURITY CLASSIFICATION OF THIS PAGE(When Data Entered)

19. KEY WORDS (Continued)

20. ABSTRACT (Continued)

normals of approximately 63° . A relativistic cyclotron-resonance analysis for the same model plasmasphere using the ray-tracing results gives an energy vs L-shell dependence for the precipitated electrons which is in excellent agreement with the observed dependence. The VLF transmitter is most likely the UMS transmitter located near Gorki, U.S.S.R. It transmits on 17.1 kHz.

VLF records covering this frequency band were available for only three of the time periods when electrons were observed. In two cases UMS was transmitting at the time period required to account for the observations. In the third case a higher frequency is required to fit the data. At the time, the NWC transmitter at North West Cape, Australia was operating at 22.3 kHz. These data are consistent with a model in which weak pitch-angle scattering by whistler-mode waves from NWC does not completely fill the drift loss cone at the longitude of NWC.

Accession For	
NTIS GRA&I	<input checked="" type="checkbox"/>
DDC TAB	<input type="checkbox"/>
Unannounced	<input type="checkbox"/>
Justification	
By _____	
Distribution/	
Availability Codes	
Dist.	Avail and/or special
A	

UNCLASSIFIED

SECURITY CLASSIFICATION OF THIS PAGE(When Data Entered)

CONTENTS

PREFACE.....	3
INTRODUCTION.....	5
RAY TRACING ANALYSIS.....	9
RESONANCE CALCULATIONS.....	10
COMPARISON OF VLF TRANSMISSIONS AND PARTICLE DATA.....	19
A SUCCESSFUL PREDICTION.....	33
WAVE-INTENSITY ESTIMATE.....	37
CONCLUSIONS.....	43
REFERENCES.....	45

FIGURES

1. Electron Flux vs. Time Plots of Data Obtained in the Drift Loss Cone by the OVI-19 Satellite in 1969.....	7
2. Cartoon Presenting the Interaction of Coherent Waves from a Ground Based Transmitter with Electrons Near the Geomagnetic Equator.....	8
3. Equatorial Electron Density as a Function of L Calculated Using a Diffusive-Equilibrium Model and the Base Densities Shown.....	11
4. Wave-Normal Angle at the Equator, Assuming Unducted Propagation, for the Three Models of Fig. 3.....	12
5. Equatorial Pitch-Angle as a Function of L for Particles in the Local Bounce Loss Cone and Stable Trapping Zone.....	14
6. Plot of Energy vs. L for the Peak Intensity of the Data of Fig. 1.....	15

FIGURES (Continued)

7.	Data Similar to Fig. 6, but Includes all of the Events Identified in the OVI-19 Data Set.....	17
8.	Plot Similar to Fig. 7, but Using the Data of Imhof et al. (1974 a,b).....	18
9.	Data Similar to Fig. 1, for August 15, 1969.....	21
10.	Plot Similar to Fig. 6, but for the data of Fig 9.....	22
11.	Traceback in Time and Longitude of Electrons Observed by the OVI-19 Satellite on August 15, 1969.....	24
12.	Data Obtained at Higher Altitude Just Prior to That Shown in Figs. 9-11.....	27
13.	Presentation Similar to Fig. 11, but for Data Obtained on August 14, 1969.....	29
14.	Presentation Similar to Fig. 11, but for Data Obtained on the Second Pass of August 15, 1969.....	31
15.	Idealized Equatorial Pitch-Angle Distribution of Electrons Which Interact with the Atmosphere at the South Atlantic Anomaly.....	36

TABLES

1.	VLF Transmitters Identified in Byrd Antarctica VLF Data on August 15, 1969.....	25
2.	Parameters Used to Calculate the VLF Transmitter Frequency for the Observations at 22:18 UT on August 15, 1969.....	34
3.	Parameters Used in the Pitch-Angle Diffusion Calculation.....	41

PREFACE

The authors are indebted to Michael Schulz who derived the expressions for pitch-angle scattering used in this paper.

This work was supported in part by the Atmospheric Research Section of the National Science Foundation under Grant ATM 77-28187 and in part by the Space Division of the U.S. Air Force under Contract F04701-80-C-0081.

Introduction

Recent low-altitude satellite measurements of electrons in the drift loss cone between $L \sim 1.6$ and $L \sim 1.8$ display several characteristics which suggest that the electrons were precipitated by a resonant interaction with waves from a ground-based VLF transmitter [Vampola and Kuck, 1978; Imhof et al. 1974a, b]. The easternmost edge of the pitch-angle scattering region can be determined from the size of the observed loss cone in the particle pitch-angle distribution under the following assumptions (1) the pitch-angle scattering is sufficiently strong to fill the drift loss cone to at least the edge of the local bounce loss cone, (2) the atmosphere removes all particles which have a mirror altitude below 100 km at the location where they have been pitch-angle scattered down from higher mirror altitudes and (3) that no further scattering occurs as the particles drift eastward. Using the observed value of the loss-cone angle of electrons in the drift loss cone, Vampola and Kuck [1978] showed that the particles could be mapped westward in longitude to the region in which they were precipitated (see Vampola and Kuck [1978] for a discussion of this mapping procedure and the limits of accuracy). For precipitation events in the L range from 1.6 to 1.85, they found that most of the events mapped back to a small region of longitude near 60° E. Assuming a density model with a L^{-4} dependence and ducted propagation, Imhof et al. [1974a, b] found that the particles they observed could resonate with ducted waves at a frequency of 10 kHz, which is very close to the lowest frequency used by the world-wide Omega navigation transmitters at 10.2 kHz. However the authors did not make a positive identification of the source of the waves, nor did they show that such ducted waves occurred in this region of the plasmasphere.

The measurements reported by Vampola and Kuck [1978] and by Imhof et al. [1974a, b] have the following characteristics in common: all of the observations exhibit

a very narrow energy distribution and the energy decreases with increasing L-shell. An example from the OV1-19 data is shown in Fig. 1. Furthermore, Vampola and Kuck [1978] using high-resolution pitch-angle data show that the particles entered the drift loss cone in a narrow longitude range which was typically just to the west of 60° E. The first and second characteristics suggest that there was a resonant interaction with a monochromatic signal. The third characteristic indicates that the signal was generally confined to one locality on the ground, presumably a VLF transmitter in the Soviet Union. In this paper we investigate the resonant interaction with a ray-tracing analysis and use data from a ground-based VLF receiver to show that the sources of the waves were the VLF transmitter UMS located near Gorki, USSR and the NWC transmitter located at North West Cape, Australia.

Figure 2 shows a diagram of the interaction mechanism in the inner magnetosphere. A ground-based VLF transmitter at a midlatitude location excites VLF waves which propagate worldwide in the earth-ionosphere waveguide. Some of the VLF energy couples into the ionosphere and enters the magnetosphere where both ducted and nonducted propagation takes place. The maximum intensities in the magnetosphere occur near the longitude of the VLF transmitter. The nonducted rays entering between the magnetic dipole latitudes of 23° and 31° cross the magnetic equator between $L \sim 1.5$ and $L \sim 1.8$ with wave-normal angles near 63° with respect to the magnetic-field direction. In a region about the equator these VLF waves can interact with 100 to 500 keV electrons by a doppler-shifted cyclotron resonance. Pitch-angle scattering resulting from the resonance process will cause the electrons to be precipitated into either the drift loss cone or the local bounce loss cone where they can be observed by a low-altitude satellite such as OV1-19.

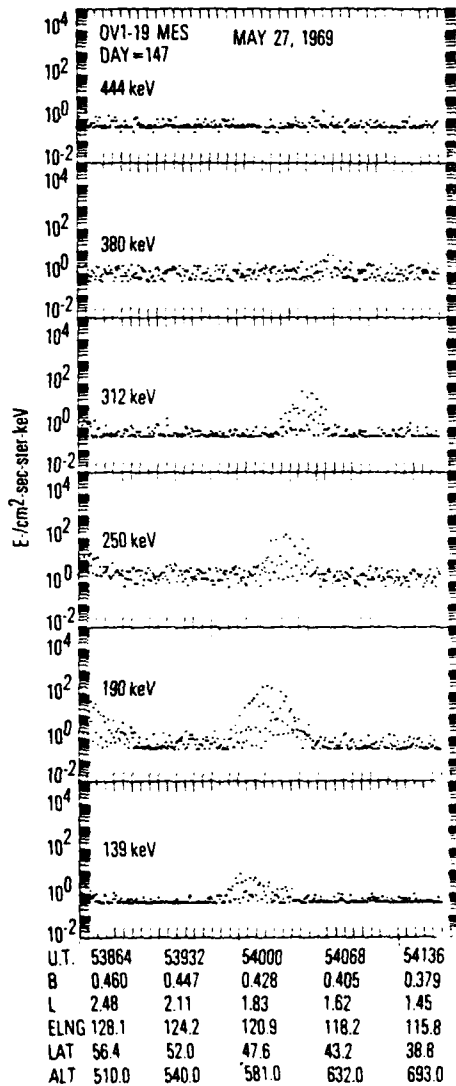


Fig. 1. Electron Flux vs. Time plots of data obtained in the drift loss cone by the OV1-19 satellite in 1969. The location of the peak in L increases monotonically with decreasing electron energy. The scatter in data points is due to pitch-angle sampling.

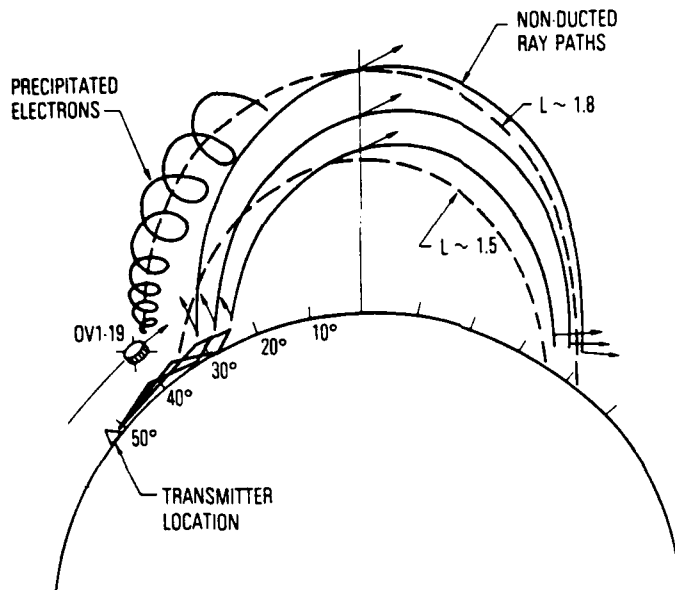


Fig. 2. Cartoon presenting the interaction of coherent waves from a ground based transmitter with electrons near the geomagnetic equator. Waves from the transmitter propagate southward in the ionospheric cavity and leak up through the ionosphere to the equatorial region where they interact with northward travelling electrons. The electrons lose perpendicular momentum to the waves, thereby lowering their pitch-angles. Some are lost into the atmosphere; the remaining electrons then have a pitch-angle distribution which is characteristic of the location at which the atmospheric interaction occurred. The distribution is then observed by a low altitude satellite, such as OV1-19, as the electrons drift eastward to the South Atlantic Anomaly (where the distribution is changed back to that characteristic of the SAA).

Ray Tracing Analysis

There are several reasons why nonducted propagation is assumed instead of ducted propagation. Examining the doppler shifts of waves from a VLF transmitter arriving in the topside ionosphere of the conjugate hemisphere Cerisier [1974] and Edgar [1976] found that below $L \sim 2$ all satellite observations can be satisfactorily explained by nonducted propagation. Ground-based observations of low L-shell whistlers are highly dependent upon magnetic storms for the production of density gradients necessary for the proper ducting of the ray paths [Singh, 1976]. All of the observations reported by Vampola and Kuck [1978] occurred during magnetically quiet or moderately disturbed ($K_p < 3$) conditions under which the density structures producing whistler-mode ducts are not likely to exist. Thus, nonducted VLF propagation is the assumed mode for $L < 2$.

Although observed far to the east of the transmitter, the electrons were presumably precipitated near the longitude of the transmitter where its signal strength in the magnetosphere would be strongest. The electrons then drift eastward at a rate which depends upon their energy, equatorial pitch angle and L-shell. The electrons observed by the satellite in a very short span of time (typically ~ 30 sec for the data as shown in Fig. 1) were in fact precipitated more than an hour earlier with the lower-energy particles precipitating tens of minutes before the higher-energy particles. Detailed calculations are presented below.

VLF ray-tracing calculations were performed for a model plasmasphere in diffusive equilibrium [Angerami and Thomas, 1964]. The diffusive-equilibrium model used a 90 to 10 percent H^+ to O^+ mixture at 1600° K at 1000 km. The model is parameterized by the electron density at 1000 km. The ray-tracing calculations were done for densities

at 1000 km of 5×10^3 , 10^4 , and $2 \times 10^4 \text{ cm}^{-3}$. The solid lines in Fig. 3 show the L-shell profile of the electron density at the magnetic equator for these models.

Assuming that the interaction between the particles and the nonducted waves occurs at the equator, the important parameter for the resonance calculation determined from the ray-tracing analysis is the wave-normal angle of the whistler-mode wave in the interacting region. The wave-normal angle at the equator determined for the three models is shown in Fig. 4. The wave-normal angle lies between 62 and 64° and is essentially independent of the model density over most of the L-shell range of interest.

Resonance Calculations

An electromagnetic wave propagating in the whistler mode resonates with electrons in the inner zone through the doppler-shifted cyclotron resonance. The general resonance condition is

$$\omega - \vec{k} \cdot \vec{v} = m\Omega \quad (1)$$

where ω is wave frequency, k is the wave vector, v is the electron velocity, m is the order of the resonance, and Ω is the electron cyclotron frequency. For the first-order cyclotron resonance for relativistic electrons this equation may be rewritten

$$\omega(1 + \beta \mu \cos \theta \cos \alpha) = \Omega (1 - \beta^2)^{1/2} \quad (2)$$

where $\beta = v/c$, α is the electron pitch angle, θ is the wave normal angle, and μ is the index of refraction for the whistler mode.

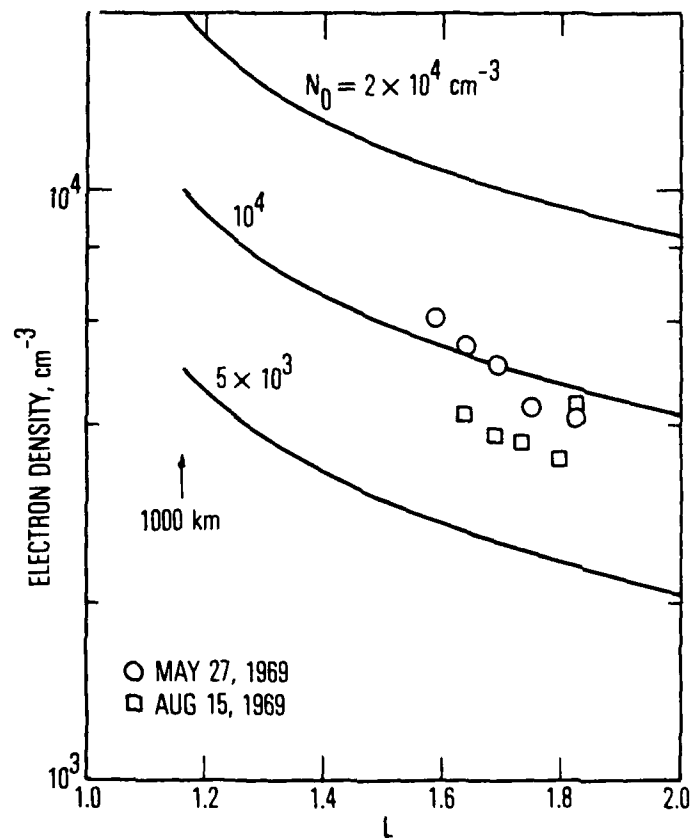


Fig. 3. Equatorial electron density as a function of L calculated using a diffusive-equilibrium model and the base densities shown. Electron densities for two electron precipitation events are plotted as squares and circles. See text for details.

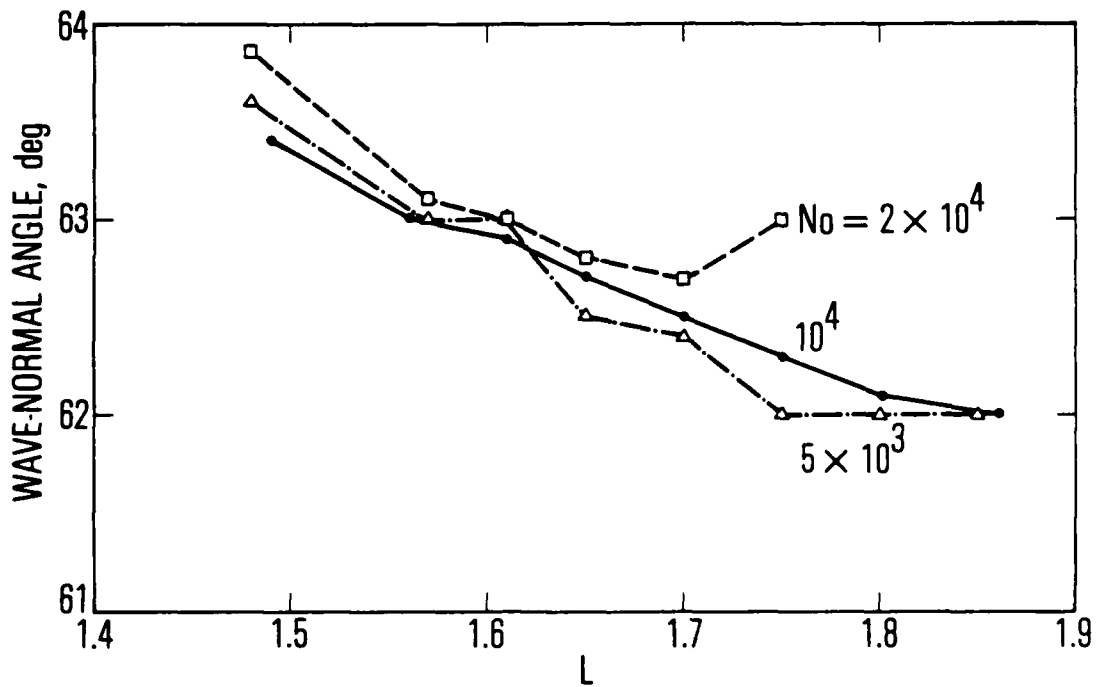


Fig. 4. Wave-normal angle at the equator, assuming unducted propagation, for the three models of Fig. 3. The angle is essentially independent of the base density assumed.

The index of refraction, which is the ratio of the velocity of light to the phase velocity of the wave, may be written

$$\mu = [1 + \frac{\omega_p^2}{\omega(\Omega_o \cos \theta - \omega)}]^{1/2} \quad (3)$$

where $\omega_p^2 = Ne^2/m_o \epsilon_o$. The electron plasma frequency depends only on the electron density, N, in the diffusive equilibrium model of the plasmasphere.

For an interaction at the magnetic equator with a specific frequency $f = \omega/2\pi$ on a given L-shell which determines Ω_o , with waves of wave-normal angle θ which is determined from the ray-tracing calculations and is a function of L, Eq. 2 is a relationship between the particle energy which is determined by β , its pitch angle α and the electron density through ω_p .

The equatorial pitch angle used in the resonance calculation is the pitch angle at the edge of the stable-trapping region. This represents particles which have just survived an azimuthal drift through the South Atlantic Anomaly. As shown in Fig. 5 the pitch angle that defines the limit to the stable-trapping region is a function of L.

We are finally left with a relationship between the equatorial electron density as a function of L and the energy of the corresponding resonant electrons.

Since the electrons are observed in our experiment we use Eq. 2 to compute the electron density as a function of L. The L-shell at which the particle count rate reaches a peak in each energy channel is taken to be the L-shell of the interaction for that energy. The L-shell dependence of the electron energy extracted from the data shown in Fig. 1 is shown in Fig. 6.

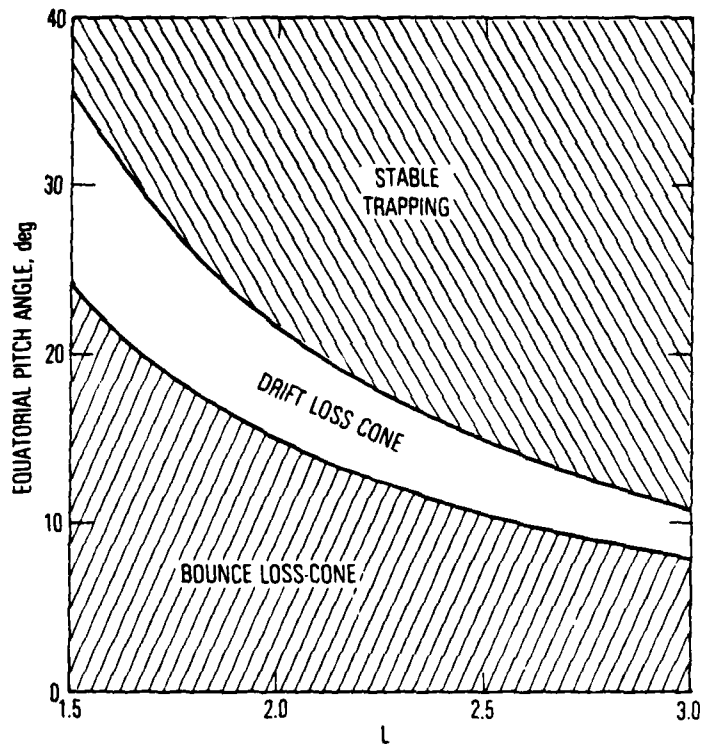


Fig. 5. Equatorial pitch-angle as a function of L for particles in the local bounce loss cone and stable trapping zone. Particles with intermediate equatorial pitch-angles, unhatched area, will mirror above the atmosphere over some portion of longitude but will encounter the atmosphere prior to completing 360° of drift.

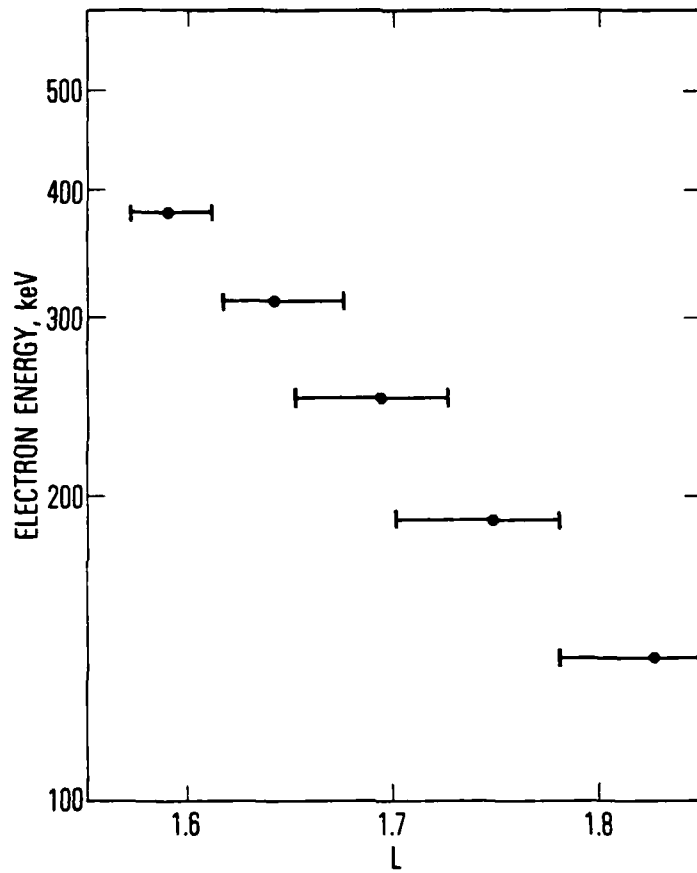


Fig. 6. Plot of Energy vs. L for the peak intensity of the data of Fig. 1.

The electron density calculated from Eq. 2 using the procedure described above is plotted as circles on the graph in Fig. 3. The data generally follow the curve which is the model for diffusive equilibrium with a base-level electron density of 10^4 cm^{-3} at 1000 km.

The L-shell dependence of the peak count rate for each energy channel for all of the events detected by satellite OV1-19 is shown in Fig. 7. The predicted energy dependence for diffusive-equilibrium models with base-level electron densities of 10^4 and $2 \times 10^4 \text{ cm}^{-3}$ at 1000 km altitude are drawn as dashed lines in Fig. 7.

The slope of the data is in excellent agreement with the slope of the predicted dependence and most of the events lie within the limits defined by these density limits. Departures from diffusive equilibrium lead to changes in the slope of the energy dependence vs L-shell curve.

Well defined peaks in the data can be used to estimate the electron density profile by the technique used above to obtain the data points shown on Fig. 3.

As mentioned earlier Imhof et al. [1974a, b] observed electrons in the drift loss cone with an energy vs L-shell dependence similar to those observed by OV1-19. We have replotted their data in Fig. 8 with bands showing the predicted energy dependence for diffusive equilibrium models with base level electron densities of 10^4 and $2 \times 10^4 \text{ cm}^{-3}$ at 1000 km for nonducted waves between 15 kHz and 18 kHz. This model gives a reasonable fit to both the magnitude and slope of the data.

Since their data was taken just west of the South Atlantic Anomaly, the particles could have been precipitated by any of the transmitters that are active in the VLF communications band.

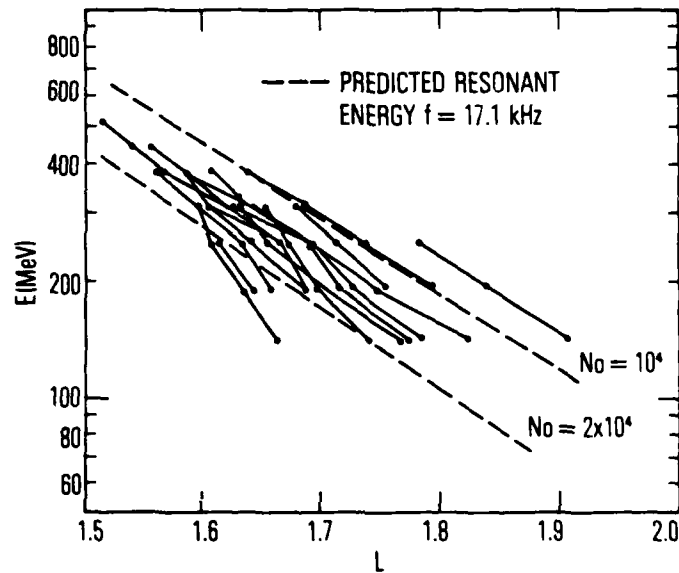


Fig. 7. Data similar to Fig. 6, but includes all of the events identified in the OV1-19 data set. The dashed lines are the result of calculations using a diffusive-equilibrium model and the procedure outlined in the text.

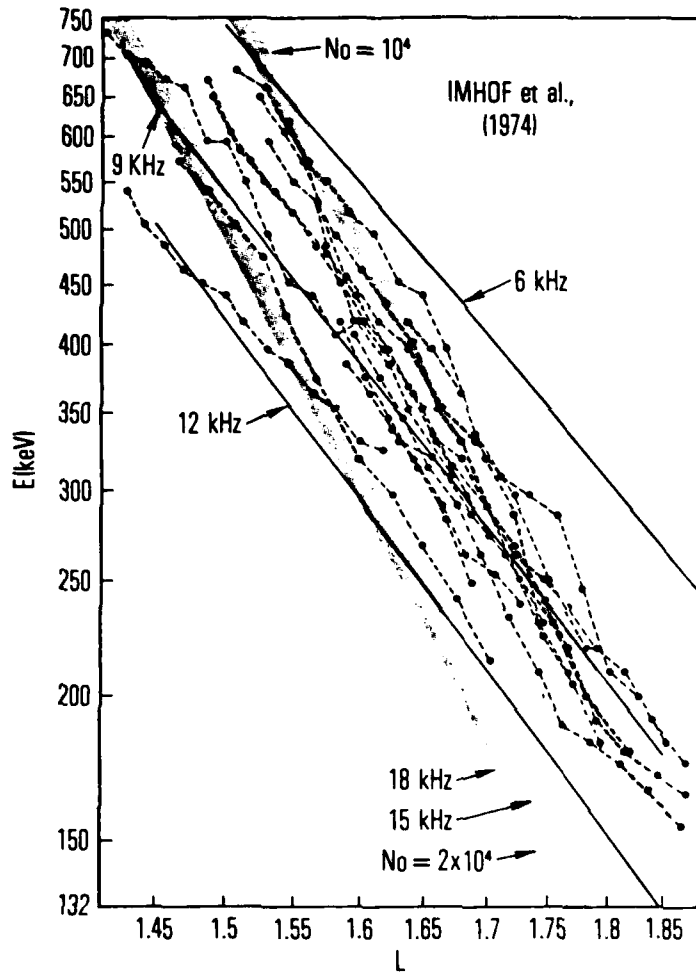


Fig. 8. Plot similar to Fig. 7, but using the data of Imhof et al. (1974a, b). Solid lines are the calculations of Imhof et al. The diffusive-equilibrium model with the procedure in the present work (grey bands) gives a better fit to the slope.

Comparisons of VLF Transmissions and Particle Data

Electrons precipitated into the drift loss cone will drift eastward until they interact with the atmosphere and are lost, usually in the region of the South Atlantic Anomaly. The rate at which they drift eastward is a function of energy, L-shell, and equatorial pitch angle.

The drift period, $2\pi/\Omega_3$, can be calculated using the formula given by Schulz and Lanzerotti [1974]:

$$2\pi/\Omega_3 = -(3L/2\pi\gamma) (\gamma^2 - 1) (c/a)^2 (m_0/qB_0) D(y)/T(y) \quad (4)$$

where γ is the relativistic mass factor, c is the velocity of light, a is the radius of the earth, m_0 is the electron rest mass, q is the electron charge, B_0 is the equatorial magnetic field at the surface of the earth, and y is $\sin \alpha$. $D(y)$ and $T(y)$ are given by:

$$T(y) \approx T(0) - 1/2 [T(0) - T(1)] (y + y^{1/2})$$

$$D(y) \approx \left\{ 4T(0) - [3T(0) - 5T(1)] y - [T(0) - T(1)] (y \ln y + y^{1/2}) \right\} / 12$$

$$T(0) \approx 1.3802$$

$$T(1) \approx 0.7405$$

The effect of the difference in drift velocity as a function of energy and L-shell will be to produce a dispersion in time for the various energy components simultaneously precipitated at the same longitude. Since the difference in drift velocity can be quite significant, the particles observed at a given longitude may have been precipitated at

widely varying times. As an example, particles observed at 120° E. can include 380 keV electrons precipitated 22 minutes earlier (assuming a precipitation at 44° E.) and 139 keV electrons precipitated 50 minutes previously. In spite of the dispersion which occurs, it is possible to attempt to correlate the precipitation with the operating schedule of the assumed transmitter, UMS.

Using the drift period obtained from Eq. 4 the particles' longitude can be traced backward in time from the longitude of the observation. The drift period is a function of the particle energy through γ , the equatorial pitch angle α through y , and the L -shell. The equatorial pitch angle is taken to be the equatorial pitch angle of electrons which are locally mirroring at the satellite in the drift loss cone at the location of the observation.

VLF recordings from Byrd Station, Antarctica (private communication, R. Helliwell) were examined for time periods when data in the drift loss cone were available from the OV1-19 satellite. There were three periods when both particle data and VLF recordings at the appropriate times were available. The time required for these electrons to drift from the assumed longitude of origin, 44° E., to the location of the satellite data, 140 to 180° E., is typically 30 minutes to an hour, the exact time depending on the total longitude through which the particles drift. Hence, the recording must actually cover some time preceding the particle observation times. The three periods occurred on August 14, 1969 at about 19:30 UT and on August 15, 1969 at about 19:45 and 22:20 UT.

The data shown in Fig. 9 were obtained at 177° E. on August 15, 1969 at about 19:45 UT. The L -shell dependence of the peaks in each energy channel is shown in Fig. 10 and the equatorial electron density obtained from the resonance analysis is plotted as squares in Fig. 3.

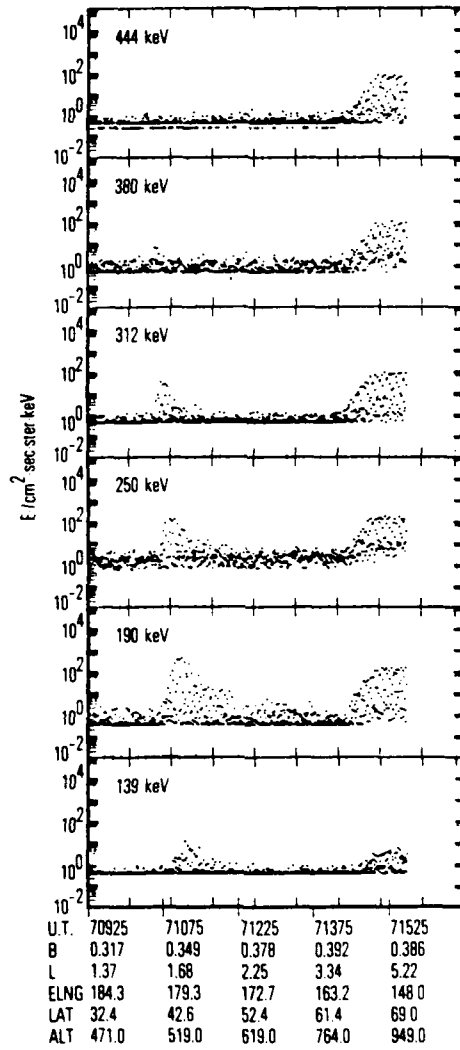


Fig. 9. Data similar to Fig. 1, for August 15, 1969.

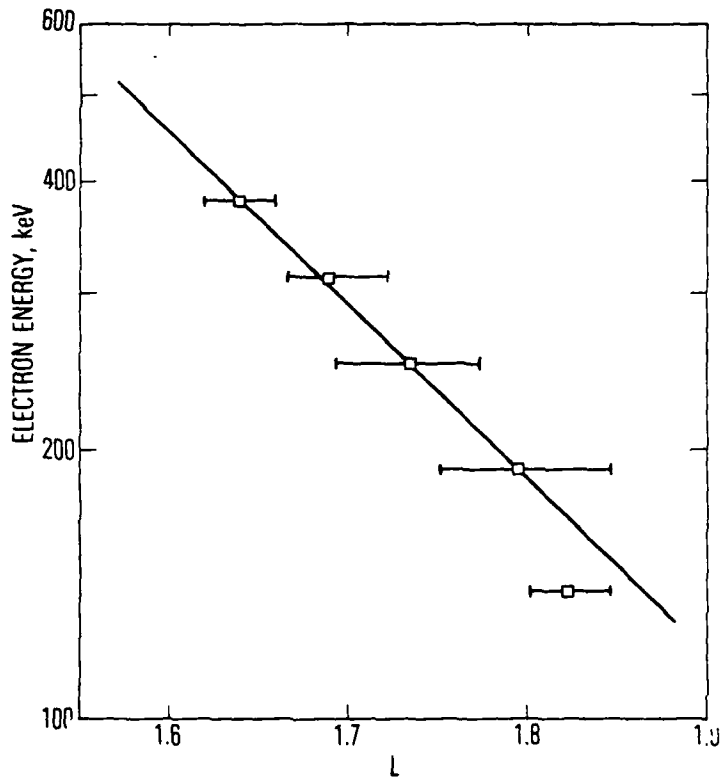


Fig. 10. Plot similar to Fig. 6, but for the data of Fig. 9.

The drift rate corresponding with each energy channel was computed from Eq. 4 for the peaks as identified in Fig. 10. The resulting longitude trace as a function of Universal Time is plotted in Fig. 11 for each energy channel. The traces converge on the longitude of the satellite, 177° E., at the time of the observation, 19:45 UT. They show the longitude of the detected particles as a function of time prior to the observation.

A VLF spectrogram covering the frequency range from 0 to 20 kHz was obtained from tape-recorded data taken at the Byrd Antarctica VLF receiver site on August 15, 1969 during the time period shown in Fig. 11. The stations identified from this record are shown in Table 1. UMS and NDT were identified by Morse Code call signs in the transmissions. The others were identified from their known transmission frequencies during August 1969. The only stations operating below 20 kHz at that time and located at longitudes between the South Atlantic Anomaly east to the satellite location were GBR, JXZ, UMS, and RPS. The signal strengths from JXZ and GBR at Byrd are very weak and the stations are located well to the west of the longitude to which the particles are traced back.

Thus UMS and RPS are the likely candidates to account for the observed electron precipitation. UMS is located near Gorki, east of Moscow, at approximately 56.2° N. and 44° E. [Watt, 1967]. The location of RPS is unknown, however Aksenov et al. [1970, 1975] report using a transmitter at 16.1 kHz at $43^{\circ} 51'$ N. and $77^{\circ} 11'$ E. for satellite experiments conducted in 1967 and 1969. We shall assume that RPS is located near 77° E. and see if this is consistent with the OV1-19 particle measurements.

We assume that the longitude width over which the interaction occurs is $\sim 15^{\circ}$ about the longitude of the station. Although somewhat arbitrary it is based upon our analysis of ground-based transmitter signals detected by a VLF receiver aboard the S3-3 satellite.

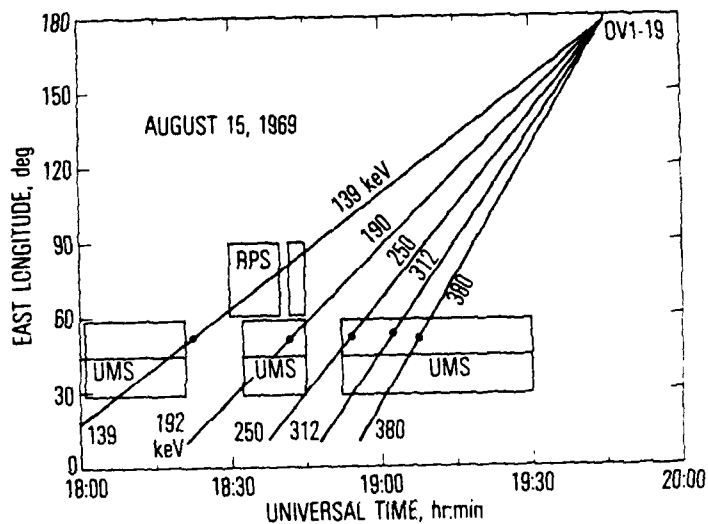


Fig. 11. Traceback in time and longitude of electrons observed by the OV1-19 satellite at about 19:45 UT on August 15, 1969, at 177° east longitude. The dots represent the longitude at which the bounce loss-cone angle matches the observed cutoff in pitch-angle in the electron distribution. The boxes marked "UMS" denote the times during which UMS was transmitting. They are centered at the presumed longitude of UMS and have a width of $\pm 15^{\circ}$ (the assumed maximum longitudinal distance over which UMS is effective in precipitating electrons).

Table 1
 VLF Transmitters Identified in Byrd, Antarctica
 VLF Data on August 15, 1969

Frequency, kHz	Station	E. Long.	N. Lat.
16.0	GBR	356.5	55.0
16.2	RPS (UMS)		
16.4	JXZ	13.0	66.4
17.1	UMS	44.0	55.8
17.4	NDT	139.5	35.7
17.8	NAA	292.7	44.7
21.4	NSS	283.6	39.0
22.3	NWC	114.2	-22.8
23.4	NPM	202.2	21.4
24.0	NBA	280.4	9.1

The operating time periods obtained from the VLF spectrograms are plotted on Fig. 11 as boxes whose abscissae cover the time periods of the transmissions and whose ordinates are $\pm 15^\circ$ about the longitude of the transmitters. Between 18:32 and 18:45 UT the transmissions from UMS and RPS are coincident in time.

The particles detected by OV1-19 at 19:45 UT must have interacted with the waves from the transmitters within the longitude-time boxes shown in Fig. 11. The traceback longitude for the particles in this model would be the longitude at which particles in a given energy channel exited from the last box they traversed. Thus from Fig. 11 the traceback longitude for the 139 keV particles would be 87° E. while all of the other energies would trace back to 59° E.

We have been concentrating on particle data obtained while the OV1-19 was in the drift loss cone since such data gives a clear upper limit to the length of time between the wave-particle interaction responsible for lowering the electron mirror points and the time of observation. However, the effects of these wave-particle interactions are also observable in data obtained at higher altitudes. Figure 12 presents data obtained at 19:24 UT just prior to that shown in Figs. 9 to 11. Here we see that electrons have been pitch-angle scattered from the stable-trapping region to lower pitch angles. Pitch angles from the stable-trapping boundary to the angle at which electrons will mirror at 100 km at the longitude of UMS are smoothly filled in. At lower angles, there is still some flux present (including fluxes in the local bounce loss cone) but the slope of the flux vs. pitch-angle curve abruptly changes. If the particles were scattered in the vicinity of UMS, this is a feature we would expect. The drift time for these electrons from 59° E. to the longitude of observation is 76 minutes. UMS was transmitting at the required time, 18:08 UT, as shown in Fig. 11.

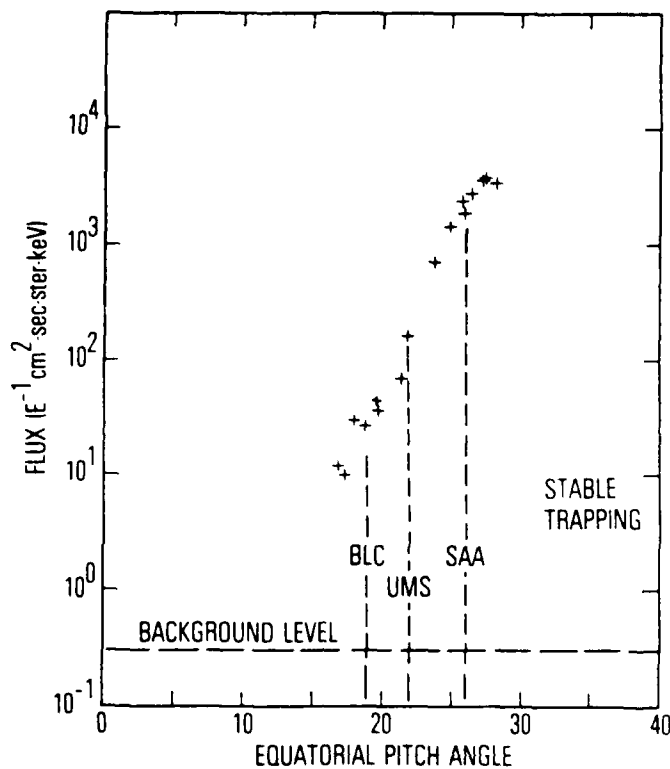


Fig. 12. Data obtained at higher altitude just prior to that shown in Figs. 9-11. Local pitch-angles have been transformed to equatorial pitch-angles for comparison with the local bounce loss cone (BLC), the bounce loss cone at the longitude of UMS (UMS) and the bounce loss cone at the field minimum at the South Atlantic Anomaly (SAA). Note that the distribution is smooth from the stable trapping angle to the "UMS" angle and drops abruptly there, as would be expected if particles were strongly pitch-angle scattered at the longitude of UMS and drifted to the longitude of observation (190°) with only small perturbations of their pitch-angles.

The data from the observation on August 14, 1969 is shown in Fig. 13 in the form of a traceback in time and longitude from the point of observation of the particles by the OV1-19 to the time and longitude of their last interaction with the atmosphere (and presumed longitude of origin). On August 14, particles were observed in only three energy channels. The transmission times of UMS, as determined from the Byrd recordings, are shown as rectangular boxes as in Fig. 11. All three channels trace back to periods of transmissions. The 250 keV channel had a poorly defined local loss-cone with a shape that indicated that a spread in longitude was contributing particles to it. The limits of this spread, as determined from the pitch-angle distribution and the altitude of the satellite (particles originating west of 48° E. would have been mirroring above the satellite), were 48° and 58° E. The 48° E. location, using a traceback energy of 250 keV, requires that the channel be responding to electrons of energies of 250 keV and below. Particles with higher energy would have already drifted past the location of the satellite. The 250 keV particles would have been precipitated by the trailing end of the third transmission. Particles with lower energies could trace back to either the same longitude at earlier times or the same time at more eastern longitudes. Particles at the nominal lower energy limit of the channel response, 225 keV, trace back to the 58° E. limit at the same time as the 250 keV electrons trace back to 48° E. Hence, the channel is responding to particles with energies in the lower half of the channel response, all of which came from the trailing end of the transmission and a spread in longitudes corresponding to the variation in drift speed. The poor loss-cone definition is the result of the easternmost edge of the precipitation region not being represented in the entire energy spread accepted by the channel. A somewhat similar effect occurs in the 192 keV channel. Here the channel is responding to the leading edge of the third transmission and the response is primarily to higher energy electrons which have drifted faster than the nominal. The lower energy particles have not yet arrived at the location of the satellite.

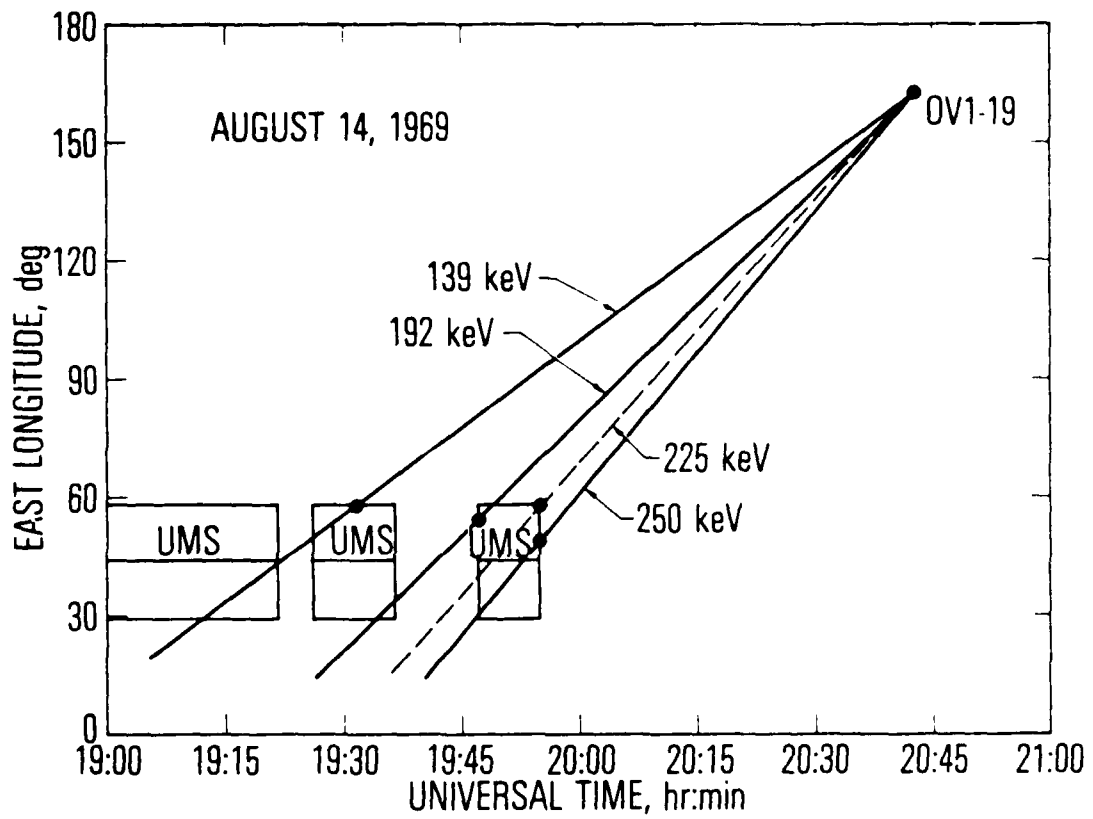


Fig. 13. Presentation similar to Fig. 11, but for data obtained on August 14, 1969.

The channel is then slightly biased to longitudes to the west of the easternmost edge of the interaction region.

The same effect, i.e., a channel responding to a particle distribution which is not uniformly represented across the entire energy response of the channel, could be the cause of the anomalous points on Figs. 3 and 10. If the 139 keV channel is responding primarily to the leading edge of the second transmission sequence (starting at 18:32 in Fig. 11), an effective energy of 160 keV results from Fig. 11. This is within the energy band of that channel. The resulting calculated points for Figs. 3 and 10 then become consistent with the rest of the points calculated for this event in those figures.

The final data set, obtained several hours after the first set on August 15, presents evidence that either multiple stations or multiple interaction regions are involved in energy-dependent (as a function of L) pitch-angle scattering. At the time these data were obtained, the OV1-19 satellite was located such that electrons pitch-angle scattered into the drift loss cone west of 58° E. should have been mirroring above the satellite and could not have been observed. Particles precipitated by UMS probably could not have been observed. However, particles were seen in the drift loss cone. The event is rather strange in that the 312 keV and 250 keV channels both peak at $L = 1.66$ and then the 250 keV and 192 keV channels both peak at $L = 1.71$. The two peaks in the 250-keV channel have different local loss-cone angles and trace back to different longitudes of origin. The 312 keV peak and the second 250 keV peak trace back to 59° E. (which is about the limit of traceback possible) while the first 250 keV peak and the 192 keV peak trace back to about 72° E. Particles were also observed in the 139 keV channel but the peak in L was not observed because data acquisition was terminated prior to the peak being reached. The data are shown on an East Longitude vs. Universal Time graph in Fig. 14. UMS was on only during the time period of the origin of the 139 keV particles. It definitely was not on during the times required for precipitation of the other energies. RPS was not on during this time period.

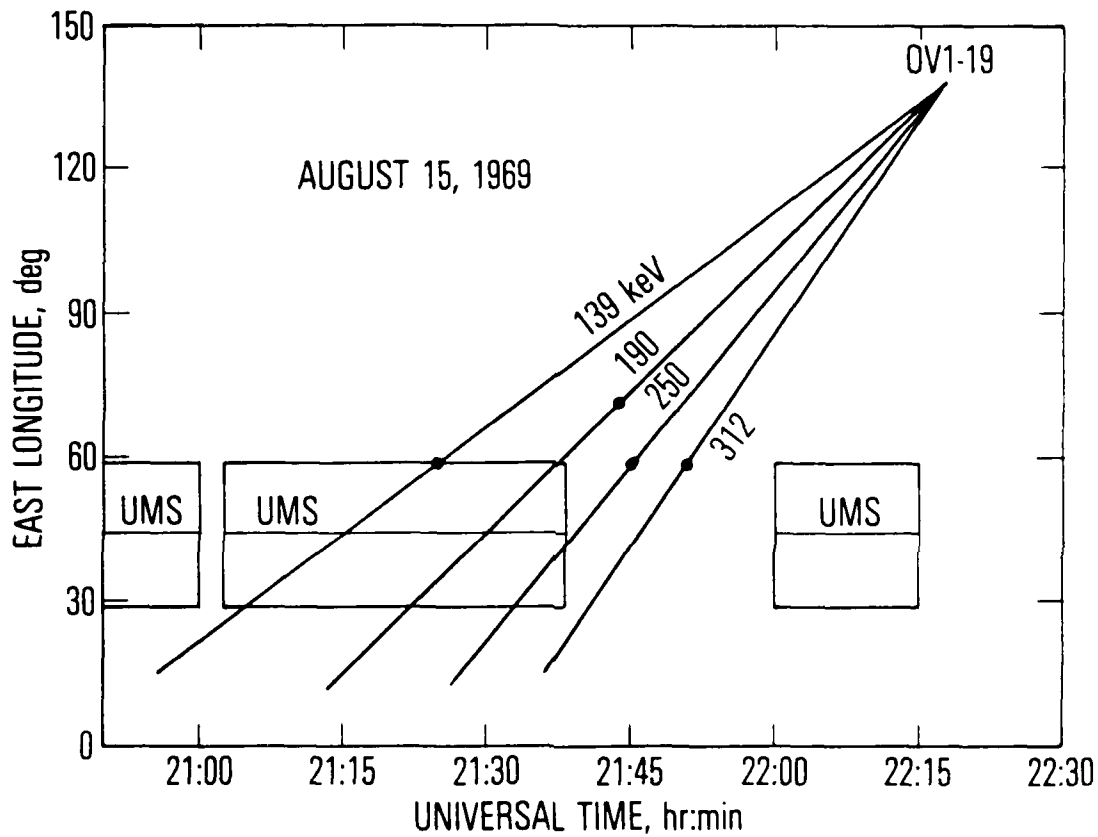


Fig. 14. Presentation similar to Fig. 11, but for data obtained on the second pass of August 15, 1969.

A SUCCESSFUL PREDICTION

Faced with the dilemma that electrons were present in the drift loss cone with the energy vs. L-shell dependence characteristic of the VLF precipitation model while it was certain that UMS was not transmitting, it was decided to invert the model in order to obtain the frequency required to fit the observations.

The observation took place one orbit, i.e., approximately 150 min, after the first event described above. The equatorial electron density for that event is plotted as squares in Fig. 3. We assumed that the density did not change between the time of the two observations and used the density profile from the earlier pass with the model to compute the frequency of the transmitter required to explain the energy vs L-shell dependence of the second observation. The electron energy, L-shell, wave-normal, and particle pitch angle (Fig. 5) were fixed. The calculations were performed for the two energies, 190 and 250 keV which have the best defined maxima. The results are shown in Table 2. The frequency required is ~ 22.0 to 22.4 kHz.

Those frequencies are above the 0 to 20 kHz range which we had requested for the spectrograms of the Byrd VLF data. We then requested a new spectrogram covering the frequency range from 20 to 25 kHz. Four transmitters were operating continuously from 20:34 to 23:15 UT. Their identities and locations are given in Table 1.

The obvious candidate to explain the observations is NWC located at North West Cape, Australia (114° E.) and operating at 22.3 kHz.

As noted above, the particles that were observed were traced back to a longitude between 59 and 72° E. There are two possible explanations for this discrepancy in longitude. The first is that the waves propagated westward in the earth-ionosphere wave

Table 2
 Parameters Used to Calculate the VLF Transmitter Frequency
 for the Observations at 22:18 UT on August 15, 1969

Energy	Equatorial Pitch Angle	L	Equatorial Electron Density	Wave Normal Angle	Frequency
190 keV	28.5°	1.713	3850 cm ⁻³	62.5°	22.4 kHz
250	30.0	1.662	4050	62.5	22.0

guide entering the magnetosphere and in fact interacting with the particles between 59° and 72° E. Insofar as signals from the high power transmitters have been observed worldwide by the OGO satellites [Heyborne, 1966], this is a possibility. The alternative explanation is depicted in Fig. 15. In Fig. 15a the solid curve shows the pitch-angle distribution of stably-trapped particles. When the interaction with a transmitter signal is strong the precipitated particles fill the drift loss cone to the edge of the bounce loss cone in the appropriate longitude range of the transmitter. The example in Fig. 15a is the one typically observed where UMS fills the loss cone at longitudes west of 60° E., similar to Fig. 12.

In Fig. 15b the solid curve again represents the pitch-angle distribution of the stably-trapped particles. If there is no interaction to the west of NWC and if the interaction with the whistler-mode waves is weak in the sense that it does not fill the local drift loss cone at NWC (in the example in Fig. 15b it fills only to 24° which is identical to the case in Fig. 15a) then the location of the interaction region in longitude cannot be determined. A priori there is no compelling reason to believe that the pitch-angle scattering must always fill the drift loss cone up to the bounce loss cone. The evidence from the resonance calculations is that NWC was the source for the waves that precipitated the particles observed at 22:45 UT on August 15, 1969. It seems more likely that weak pitch-angle scattering near the longitude of the transmitter rather than propagation in the waveguide well to the west of the transmitter is the more satisfactory explanation for the pitch-angle distributions observed.

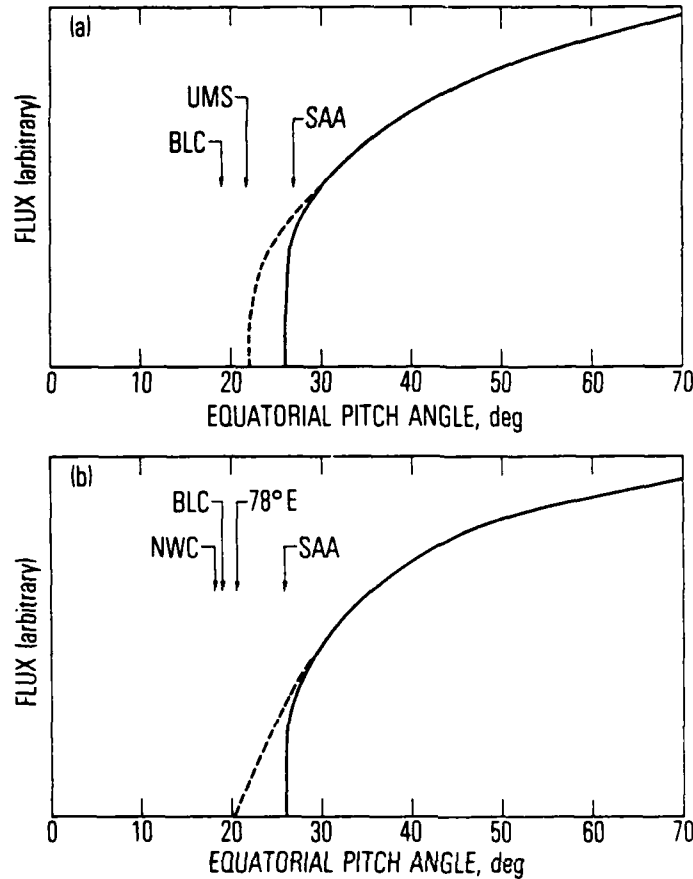


Fig. 15. a) Idealized equatorial pitch-angle distribution of electrons which interact with the atmosphere at the South Atlantic Anomaly (SAA) and are not strongly scattered by waves (solid line); modification to pitch-angle distribution which occurs if strong pitch-angle scattering occurs in the vicinity of UMS (dashed line). BLC is the bounce loss cone at the longitude of observation and, for this example, is assumed to be smaller than that at the longitude of UMS (a requirement for traceback).

b) Solid line is the same as in a), above. The dashed line represents the modification in pitch-angle that would be expected if relatively weak pitch-angle scattering (i.e., insufficient to isotropize the distribution at the location of the interaction) occurred at the longitude of the transmitter NWC (which has a local bounce loss cone smaller than the bounce loss cone at the longitude of observation).

WAVE-INTENSITY ESTIMATE

We can estimate the pitch-angle diffusion coefficient from the particle data. An estimate of the wave intensity required to account for the observed scattering can then be obtained.

The pitch-angle diffusion coefficient $D_{\alpha\alpha}$ is defined as

$$D_{\alpha\alpha} = \langle (\delta\alpha)^2 \rangle / 2\tau \quad (5)$$

where $\delta\alpha$ is the pitch angle change during a single interaction and τ is the average time between interactions [Ashour-Abdalla, 1972]. In our case $\tau = \tau_b$, the electron bounce period. The pitch angle change is averaged over all initial phases between the wave magnetic-field vector and the component of the electron velocity vector.

The change in pitch angle $\delta\alpha$ that occurs during a single interaction of duration δt is [Michael Schulz, private communication, 1980]

$$\begin{aligned} (\delta\alpha)_{\text{rms}} = & \frac{1}{\sqrt{2}} (qc/\mu p) b_{\perp} \left\{ (iR) J_{\ell}'(\zeta) \cos\alpha \right. \\ & + (\ell/\zeta) [RS \sin\theta - \cos\theta] J_{\ell}(\zeta) \cos\alpha \\ & + [RS \cos\theta + \sin\theta] J_{\ell}(\zeta) \sin\alpha \left. \right\} \delta t \\ & + \frac{1}{\sqrt{2}} (q/\gamma m) b_{\perp} \left\{ (\ell/\zeta) J_{\ell}(\zeta) \right. \\ & \left. - (iR) J_{\ell}'(\zeta) \cos\theta \right\} \delta t \quad (6) \end{aligned}$$

where q is the charge on the particle (for numerical evaluation the sign is negative for electrons), c is the speed of light, μ is the index of refraction of the wave, p is the momentum of the particle, $R = E_x/E_y$ is the polarization of the wave-field, $S = E_z/E_x$, θ is the wave-normal angle and α is the particle pitch angle (both θ and α are measured from the positive direction of the geomagnetic field; thus $\cos\theta$ in our case is negative), b_1 is the magnetic field intensity of a monochromatic wave, and l is the order of the resonance. $l = +1$ satisfies the particle observation. $\zeta = k_1 p_1 / m\Omega$ where k_1 is the component of the wave vector perpendicular to the geomagnetic field B , p_1 is the component of the particle momentum perpendicular to B , m is the relativistic mass of the particle and Ω is the gyrofrequency of the particle. We use the sign conventions of Ratcliffe [1959] where the sign of Ω is negative for electrons. For the whistler mode

$$iR \approx \text{sgn} [(\Omega_0/\omega) \cos\theta]$$

$$S \approx \frac{i (\omega_p/\omega)^2 \Omega_0 \sin\theta}{[1 - (\omega_p/\omega)^2] (|\Omega_0 \cos\theta| - \omega)}$$

where Ω_0 is the gyrofrequency for a nonrelativistic electron, $\omega/2\pi$ is the wave frequency and ω_p is the plasma frequency.

Eq. 6 is a generalization for nonzero wave-normal angle for Eq. 2.46 in Schulz and Lanzerotti [1974]. The computation assumes a linear interaction. Inan et al. [1978] has computed the non-linear pitch-angle scattering of energetic electrons by coherent VLF waves propagating with zero wave-normal angle.

The wave field required to scatter a particle can be calculated from Eqs. 5 and 6 with appropriate estimates for $D_{\alpha\alpha}$ and δt .

The diffusion time τ_D required for the pitch angle to scatter through a total change of $\Delta\alpha$ is

$$\tau_D = \langle (\Delta\alpha)^2 \rangle / 2 D_{\alpha\alpha} \quad (7)$$

The observed change in $\Delta\alpha$ is about 3 deg or 0.05 radians. A 250 keV electron with a pitch angle of 28 deg has a bounce period of 0.2 s. It drifts across the 30 deg longitude sector of the interaction region in about 300 s. Taking $\tau_D = 300$ s and $\Delta\alpha = 0.05$ we obtain from Eq. 7 $D_{\alpha\alpha} = 1.39 \times 10^{-6} \text{ s}^{-1}$.

δt is related to the intrinsic bandwidth owing to the inhomogeneity in the magnetic field [Schulz, 1972]. For equatorial cyclotron resonance the intrinsic bandwidth is $\Delta\omega/2\pi$, where $\Delta\omega$ is given [M. Schulz, 1974, 1975] by

$$\Delta\omega = |\pi^2 \ddot{\omega}/2|^{1/3} [1 - (v_{\parallel}/\hat{k} \cdot v_g) \cos \theta]^{-2/3} \quad (8)$$

where

$$\ddot{\omega} = \frac{(3c/\omega_p L_a)^2 (\Omega/\gamma - \omega)^3 [\omega(v+1 - \sec^2 \alpha) + \Omega(2/\gamma - v \cos \theta - \sec^2 \alpha \cos \theta)]}{2\omega \cos^2 \theta [1 - (v_{\parallel}/\hat{k} \cdot v_g) \cos \theta]}$$

and

$$[1 - (v_{\parallel}/\hat{k} \cdot v_g) \cos \theta] = 1 + (\Omega/\gamma - \omega) \Omega \cos \theta / 2\pi (\Omega \cos \theta - \omega)$$

for the case of electron-cyclotron resonance for a relativistic electron with a whistler-mode wave with a wave-normal angle of θ with respect to B. The cold-plasma density is taken as proportional to B^{ν} . The "gyrofrequency model" used in this paper corresponds to $\nu = 1$. The factor in brackets on the right hand side of Eq. 8 is a correction to Eq. 4 of Schulz [1972].

To a stationary observer the length of a wave train that can interact with the particle is $\delta t [1 - (v_{\parallel}/\hat{k} \cdot v_g) \cos \theta]$ in time. The interaction time δt is related to the bandwidth $\Delta\omega/2\pi$ by

$$\Delta\omega/2\pi = (\delta t)^{-1} [1 - (v_{\parallel}/\hat{k} \cdot v_g) \cos \theta]^{-1} \quad (9)$$

For the parameter values given in Table 3 the interaction time δt obtained from Eq. 9 using Eq. 8 to compute $\Delta\omega$ is 2.4 ms. The wave magnetic-field intensity computed using Eqs. 5 and 6 is then 3×10^{-12} T or 3 mY.

We can estimate the magnetic field intensity of the waves at the equator using the simple analytic method outlined by Heyborne [1966]. For an input magnetic latitude of 30° the nighttime D-region loss is 5 db, and the divergence loss is 7 dB. Assuming a radiated power for UMS of 300 kW [Watt, 1967], one obtains at $L = 1.8$ a field intensity of 4 mY for

Table 3
Parameters used in the pitch-angle
diffusion calculation

Equatorial Electron Density, n_e	=	3756 cm ⁻³
L-shell parameter, L	=	1.734
Electron Pitch Angle, α	=	28 deg
Wave Frequency, $\omega/2\pi$	=	17.1 kHz
Wave Normal Angle, θ	=	152.4 deg
Energy of Resonant Electrons, T	=	250 keV
Geomagnetic Field Intensity, B	=	5.75 × 10 ⁻⁶ T
Electron Gyrofrequency, Ω_0	=	1.01 × 10 ⁶ rad/s
v/c , β	=	0.7409
Electron Bounce Period, τ_b	=	0.2 s
Diffusion Coefficient, $D_{\alpha\alpha}$	=	1.32 × 10 ⁻⁶ s ⁻¹
Intrinsic Bandwidth, $\Delta\omega/2\pi$	=	93 Hz
Wave Index of Refraction, μ	=	17.6
Wave Group Velocity, v_g	=	2.63 × 10 ⁷

an all land path. However, in the daytime, the D-region attenuation is 35 dB, which reduces the wave intensity to 0.1 milligamma.

CONCLUSIONS

Electrons observed in the drift loss cone by the OV1-19 satellite between $L = 1.5$ and 1.8 were pitch-angle scattered by whistler-mode waves from high-powered ground-based VLF transmitters.

During three time periods on August 14 and 15, 1969 it has been shown that radiation from the VLF transmitters UMS and NWC interacting with electrons and thereby precipitating them into the drift and bounce cones, explains in a consistent manner certain particle observations. In two cases the interaction with UMS was sufficiently strong to fill the drift loss cone to the edge of the local bounce loss cone at the longitude of the interaction. In the other case the interaction with radiation from NWC did not completely fill the drift loss cone.

REFERENCES

- Aksenov, V. I., B. A. Dubinskii, L. A. Zhekulin, Z. Ya. Kiseleva, I. V. Lishin, V. A. Makarov, and L. N. Mikhailov; Investigation of transmission of ultralong radio waves through the earth's ionosphere: Preliminary results from Cosmos 142 satellite, Cosmic Res. USSR, Engl. Transl., 8, 527, 1970.
- Aksenov, V. I., Investigation of the propagation of very long waves in the earth's ionosphere, II, Results of Experiments with the Kosmos-142 and Kosmos-259 artificial satellites, Izv. Vyssh. Uchebn. Zaved., Radiofiz, Engl. Transl., 18, 996, 1975.
- Angerami, J. J. and J. O. Thomas, Studies of planetary atmospheres, 1, The distribution of electrons and ions in the earth's exosphere, J. Geophys. Res., 69, 467, 1964.
- Ashour-Abdalla, M., Amplification of whistler waves in the magnetosphere, Planet. Space Sci., 20, 639, 1972.
- Cerisier, J. C., Ducted and partly ducted propagation of vlf waves through the magnetosphere, J. Atmos. Terr. Phys., 36, 1443, 1974.
- Edgar, B. C., The theory of vlf Doppler signatures and their relation to magnetospheric density structure, J. Geophys. Res., 81, 3327, 1976.
- Imhof, W. I., E. E. Gaines, and J. B. Reagan, L dependent peaks in the energy spectra of electrons precipitating from the inner belt, in Magnetospheric Physics, edited by B. M. McCormac, D. Reidel, Hingham, Mass., 1974a.

- Imhof, W. L., E. E. Gaines, and J. B. Reagan, Evidence for the resonance precipitation of energetic electrons from the slot region of the radiation belts, J. Geophys. Res., 79, 3141, 1974b.
- Inan, U. S., T. F. Bell, and R. A. Helliwell, Nonlinear pitch angle scattering of energetic electrons by coherent VLF waves in the magnetosphere, J. Geophys. Res., 83, 3235, 1978.
- Heyborne, R. L., Observations of whistler-mode signals in the OGO satellites from vlf ground station transmitters, Stanford Electronics Laboratory Tech. Rept., SU-SEL-66-094, Stanford Univ., Stanford, CA, 1966.
- Ratcliffe, J. A., The Magneto-Ionic Theory and its Applications to the Ionosphere, Cambridge University Press, New York, 1959.
- Schulz, M., Intrinsic bandwidth of cyclotron resonance in the geomagnetic field, Phys. Fluids, 15, 2448, 1972.
- Schulz, M., Wave-Particle Interactions in the Magnetospheric Plasma, Aerospace Corporation Technical Report ATR-74(7420)-1, The Aerospace Corporation, El Segundo, CA, 1974.
- Schulz, M., Resonance Broadening in a Turbulent Plasma, Aerospace Corporation Technical Report SAMSO-TR-75-185, The Aerospace Corporation, El Segundo, CA, 1975.
- Schulz, M. and L. J. Lanzerotti, Particle Diffusion in the Radiation Belts, p. 67, Springer, New York, 1974.
- Singh, Birbal, On the ground observation of whistlers at low latitude, J. Geophys. Res., 81, 2429, 1976.

Vampola, A. L. and G. A. Kuck, Induced precipitation of inner zone
electrons, 1, Observations, J. Geophys. Res., 83, 2543, 1978.
Watt, A. D., VLFRadio Engineering, Pergammon, New York, 1967.

LABORATORY OPERATIONS

The Laboratory Operations of The Aerospace Corporation is conducting experimental and theoretical investigations necessary for the evaluation and application of scientific advances to new military concepts and systems. Versatility and flexibility have been developed to a high degree by the laboratory personnel in dealing with the many problems encountered in the nation's rapidly developing space and missile systems. Expertise in the latest scientific developments is vital to the accomplishment of tasks related to these problems. The laboratories that contribute to this research are:

Aerophysics Laboratory: Launch and reentry aerodynamics, heat transfer, reentry physics, chemical kinetics, structural mechanics, flight dynamics, atmospheric pollution, and high-power gas lasers.

Chemistry and Physics Laboratory: Atmospheric reactions and atmospheric optics, chemical reactions in polluted atmospheres, chemical reactions of excited species in rocket plumes, chemical thermodynamics, plasma and laser-induced reactions, laser chemistry, propulsion chemistry, space vacuum and radiation effects on materials, lubrication and surface phenomena, photosensitive materials and sensors, high precision laser ranging, and the application of physics and chemistry to problems of law enforcement and biomedicine.

Electronics Research Laboratory: Electromagnetic theory, devices, and propagation phenomena, including plasma electromagnetics; quantum electronics, lasers, and electro-optics; communication sciences, applied electronics, semiconducting, superconducting, and crystal device physics, optical and acoustical imaging; atmospheric pollution; millimeter wave and far-infrared technology.

Materials Sciences Laboratory: Development of new materials; metal matrix composites and new forms of carbon; test and evaluation of graphite and ceramics in reentry; spacecraft materials and electronic components in nuclear weapons environment; application of fracture mechanics to stress corrosion and fatigue-induced fractures in structural metals.

Space Sciences Laboratory: Atmospheric and ionospheric physics, radiation from the atmosphere, density and composition of the atmosphere, aurorae and airglow; magnetospheric physics, cosmic rays, generation and propagation of plasma waves in the magnetosphere; solar physics, studies of solar magnetic fields; space astronomy, x-ray astronomy; the effects of nuclear explosions, magnetic storms, and solar activity on the earth's atmosphere, ionosphere, and magnetosphere; the effects of optical, electromagnetic, and particulate radiations in space on space systems.

THE AEROSPACE CORPORATION
El Segundo, California